JOM
https://doi.org/10.1007/s11837-025-08081-9

TECHNICAL ARTICLE

Polyphenol-Mediated Iron Oxide Nanomaterials: Biosynthesis, Physicochemical Characterizations, and Analysis of Functional Groups

RAJIV PERIAKARUPPAN,[1,4] S.V. NANDITHA KRISHNA,[1] V. JEFRI SAMUEL,[1] JOAVAL ANTONY MARTIN,[1] DANUSREE BABU,[1] KARUNGAN SELVARAJ VIJAI SELVARAJ,[2] and NOURA AL-DAYAN[3]

1.—Department of Biotechnology, PSG College of Arts & Science, Coimbatore, Tamil Nadu 641014, India. 2.—Vegetable Research Station, Tamil Nadu Agricultural University, Palur 607102, Cuddalore, India. 3.—Department of Medical Lab Sciences, Prince Sattam Bin Abdulaziz University, 16278 Alkharj, Saudi Arabia. 4.—e-mail: rajivsmart15@gmail.com

The present study aims to extract and utilize the polyphenols of *Camellia sinensis* and *Mentha spicata* as active capping agents for the bio-fabrication of iron oxide nanoparticles (FeO NPs). Different techniques such as UV-Vis spectroscopy, FTIR spectroscopy, XRD analysis, FESEM, EDX analysis, and TGA were performed to determine the surface resonance, functional groups, size, shape, elemental composition, and thermal stability of the polyphenol-mediated FeO NPs. UV-Vis spectrum of *C. sinensis* and *M. spicata* polyphenol-mediated FeO NPs revealed significant absorption at 230 and 250 nm, indicating the formation of FeO NPs. The presence of metal oxides in the FeO NPs were verified through FTIR analysis. XRD spectra confirmed the crystalline structure of *C. sinensis* and *M. spicata* polyphenol-mediated FeO NPs. The occurrence of iron and oxygen was verified by the EDX spectra of both polyphenol-mediated FeO NPs. TGA analysis established that *C. sinensis* polyphenol-mediated FeO NPs had higher thermal stability than *M. spicata* polyphenol-mediated FeO NPs.

INTRODUCTION

Green synthesis plays a vital role in easily scalped for large-scale synthesis preparation of metal oxide nanoparticles (NPs) with significant properties over physical and chemical methods as they are environment-friendly, cost-effective, reproducible, and easily collected for large-scale synthesis.[1] NPs are ultra-fine particles that range in size from 1 to 100 nm, exhibiting unique physical[2] and chemical properties[3] that differ significantly from their bulk counterparts.[4] Due to their small size, NPs have a high surface area-to-volume ratio, which enhances their reactivity, making them ideal for various applications in medicine,[5] electronics,[6] and environmental science.[7,8] Additionally, NPs can exhibit quantum effects, such as size-dependent optical,[9] electrical,[10] and magnetic properties,[11] which are not present in larger particles.[12] The quantum behavior of NPs allows for innovations like drug delivery,[13] where NPs can be engineered to target specific cells or tissues, and in catalysis, where they can speed up chemical reactions more efficiently.[14]

Polyphenols are complex bioactive compounds with a phenol ring as the basic monomer.[15] Plants produce four types of polyphenols, namely flavonoids,[16] phenolic acids,[17] lignans[18] and stilbenes.[19] Polyphenols have various applications in the food industry,[20] particle engineering, cosmetic industry,[21] diagnostics[22] and therapeutics.[23]

(Received September 11, 2025; accepted December 22, 2025)

Published online: 13 January 2026

There are various modern methods, namely ultrasonic, microwave-assisted, and enzymatic separation to extract polyphenols from plants. The conventional extraction methods include soxhlet extraction, freeze-drying, maceration, and steam distillation. Conventional extraction methods are still used due to their high number of advantages, including simplicity and cost-effectiveness.[24]

Camellia sinensis (tea) belongs to the family of Theaceae and is the most popular beverage in the world with increasing demand for production and consumption.[25] *C. sinensis* is widely popular due to its sensory properties,[26] anti-inflammatory activity,[27] stimulating effects,[28] and potential health benefits.[29] *C. sinensis* leaves are rich in polyphenols, particularly flavonoids, which include flavanols and flavanol glycosides. In addition to polyphenols, *C. sinensis* leaves also contain caffeine, lipids, amino acids, minerals, and enzymes. Polyphenols make up 20–40% of the dry matter in young *C. sinensis* shoots and play a crucial role in determining the quality of the tea, as they are responsible for its color, flavor, and brightness. Recently, scientists have been extensively studying *C. sinensis* polyphenols due to their potential health benefits. The polyphenol content and composition of *C. sinensis* leaves can be influenced by several factors, including leaf variety, harvesting season, climate, processing method, and analytical method.[30]

Mentha spicata (mint) is one of the primary herbs utilized in food industry mainly for the aroma, flavor, and distinct medicinal properties. It is a member of the Lamiaceae family which comprises several culinary and medicinal herbs.[31] *M. spicata* holds phytochemicals which are responsible for its antiseptic, anti-allergic, anti-oxidant, and antimicrobial properties.[32] Polyphenols extracted from *M. spicata* leaves are found to have anti-oxidant properties, and it is known to be utilized in the management of various ailments like cancer, diabetes, and cardiovascular and neurodegenerative diseases.[33] Polyphenols can be used as a precursor for the synthesis of new therapeutic agents.[34]

NPs derived from plant polyphenols have a wide range of applications, such as drug delivery,[35] bioimaging,[22] tissue engineering, food preservation, environmental remediation,[36] and biofuel production. Jiménez-Rosado et al.[37] fabricated zinc oxide NPs using *Capsicum annuum* (pepper) polyphenols. Previous studies have reported the synthesis of platinum NPs using polyphenols extracted from *Terminalia chebula*.

Iron oxide NPs (FeO NPs) are tiny particles of iron, typically ranging in size from 1 to 100 nm, which exhibit unique physical and chemical properties compared to their bulk counterparts. Due to their small size, FeO NPs have increased surface area and reactivity, making them particularly noted for their magnetic properties. The properties of FeO NPs are useful in various applications, including targeted drug delivery, magnetic resonance imaging, and environmental remediation, especially in treating contaminated water through pollutant degradation, catalysis, and as a contrast agent in medical imaging.[38] The novelty of this study is fabrication of NPs using the polyphenols of *C. sinensis* and *M. spicata*, and it focuses on the extraction of polyphenols from *C. sinensis* and *M. spicata* leaves. In addition, the biofabrication and characterization of polyphenol-mediated FeO NPs were performed.

MATERIALS AND METHODS

Materials

Collection of C. sinensis and M. spicata

C. sinensis leaves were collected from collected from Nilgiris, Tamil Nadu, India, while *M. spicata* leaves were obtained from the greenhouse garden of PSG College of Arts & Science, Coimbatore, Tamil Nadu, India.

Preparation of C. sinensis and M. spicata Leaf Extract

An amount of 10 g of *C. sinensis* leaves were taken to prepare an aqueous extract by the homogenization of the leaves in 350 mL of distilled water. The homogenized extract was filtered using Whatman No. 1 filter paper. The same procedure was repeated with *M. spicata* leaves.

Phytochemical Screening of C. sinensis and M. spicata Leaf Extract

Preliminary phytochemical screening for various secondary metabolites such as tannins, saponins, reducing sugar, flavonoids, sterols, glycosides and phenols was performed with aqueous extracts of *C. sinensis* and *M. spicata* leaves using standard protocols.

Extraction of Polyphenols using C. sinensis and M. spicata Leaf Extract

The filtered extracts of *C. sinensis* and *M. spicata* leaves were lyophilized in a freeze dryer to obtain

Table I. Phytochemical screening of *C. sinensis* and *M. spicata* aqueous extract

Phytochemicals	*C. sinensis*	*M. spicata*
Saponins	–	+
Tannins	+	+
Reducing sugar	+	–
Flavonoid	+	+
Cholesterol and sterols	+	–
Glycosides	–	+
Phenol	+	+

+ positive, - negative

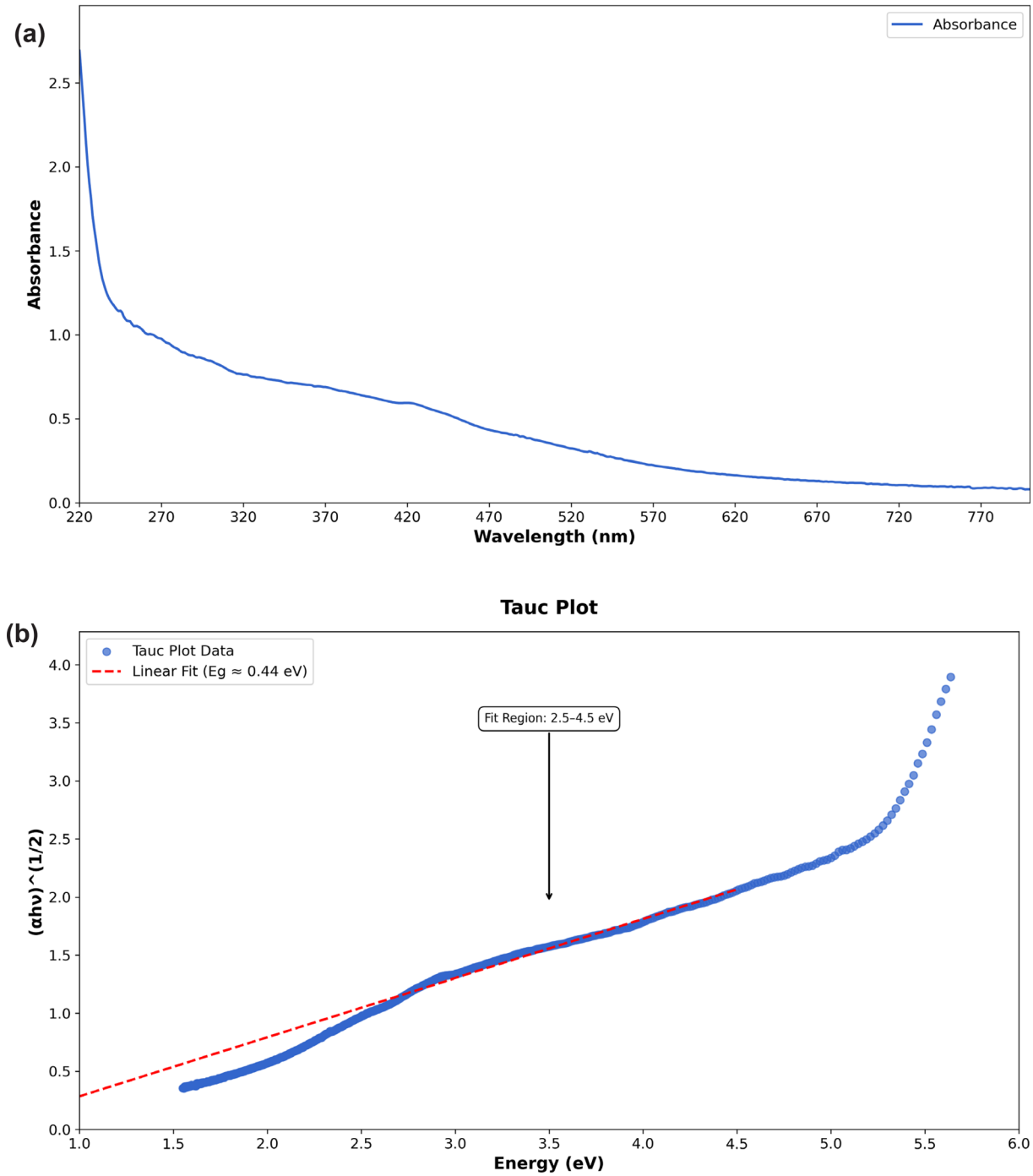

Fig. 1. (a) UV spectrum of *C. sinensis* polyphenol-mediated FeO NPs; (b) Tauc plot of *C. sinensis* polyphenol mediated FeO NPs.

polyphenol powder, which was mixed with 100 mL of distilled water and sonicated in a water bath sonicator at 400 KHz for 30 min. The extracted polyphenols from the two plants were stored in a refrigerator for further use.

Total Phenolic Content

The total phenolic content of the *C. sinensis* and *M. spicata* polyphenols was estimated using the standard protocol from Ref. 39, with the Folin-Ciocalteu reagent. The absorbance of each sample was measured at 750 nm using a UV-visible (UV-Vis) spectrophotometer (Jasco V-630), with all the measurements performed in triplicate for accuracy. A reagent blank prepared with a solvent was used as the reference during absorbance measurements. A calibration curve was constructed using the absorbance values of the standard gallic acid solutions, and the total phenolic content was calculated based on the calibration curve. Results were

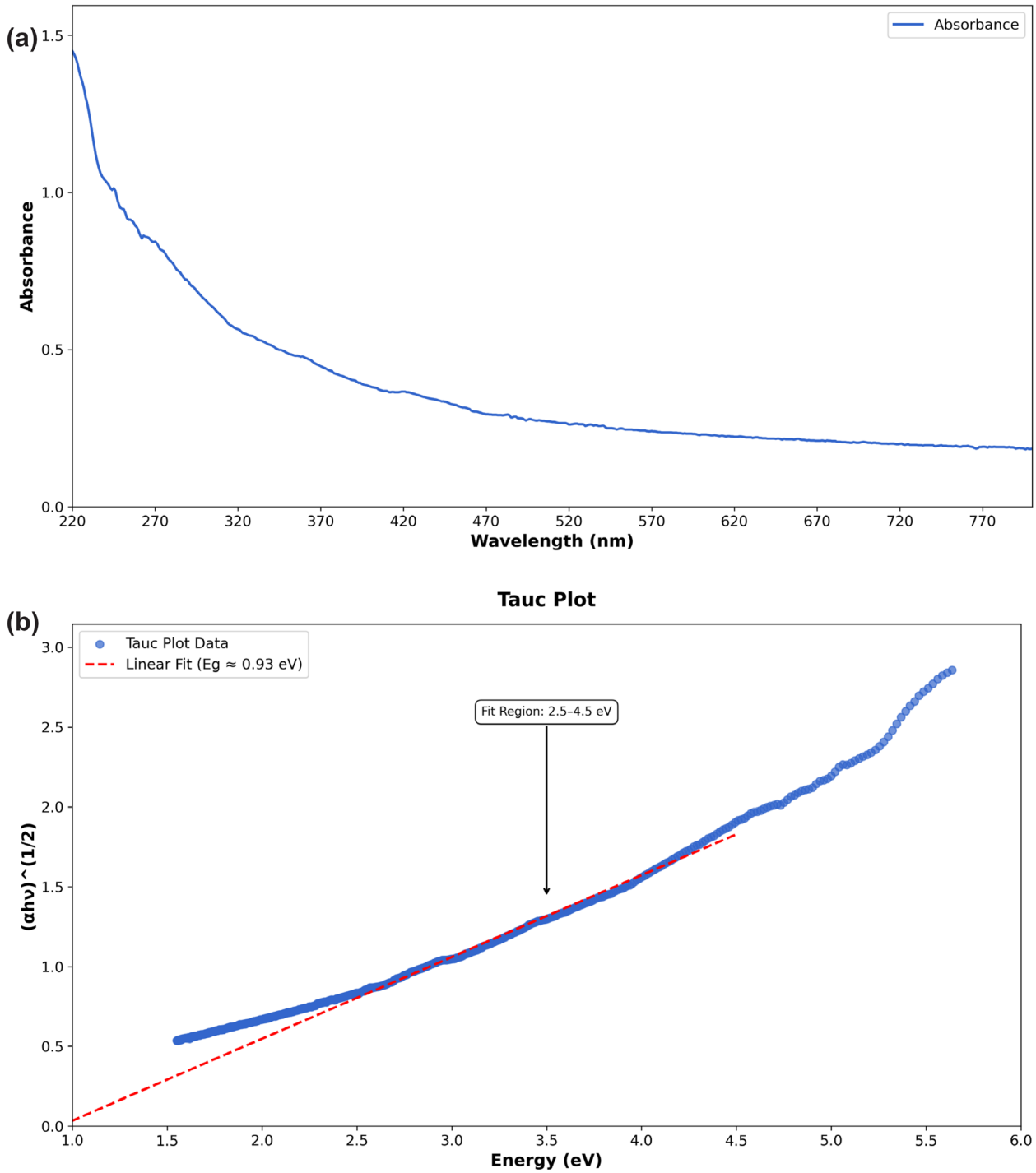

Fig. 2. (a) UV spectrum of *M. spicata* polyphenol mediated FeO NPs; (b) Tauc plot of *M. spicata* polyphenol mediated FeO NPs.

expressed as milligrams of gallic acid equivalents (GAE) per 100 grams of dry mass.

Synthesis of FeO NPs Using C. sinensis and M. spicata Polyphenols

Amounts of 50 mL of *C. sinensis* polyphenol and 50 mL of a 0.1-M ferrous sulfate precursor solution were prepared and heated in a water bath for 15 min with continuous stirring from a heat-assisted magnetic stirrer at 90 °C for 30 min. The pH of the mixture was maintained at 9. A color change of the solution from dark green to black was observed. The solution was left undisturbed overnight and the resulting precipitate was centrifuged at 10,000 rpm for 20 min and then washed with distilled water and ethanol. The supernatant was discarded, while a pellet was collected and dried in a hot air oven at 100 °C for 1 h. Similarly, fabrication

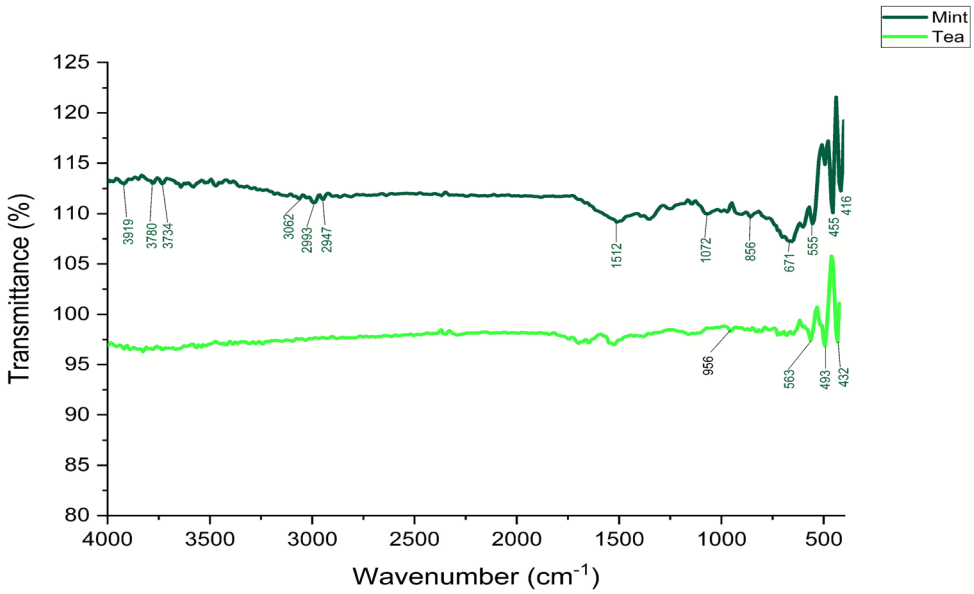

Fig. 3. FTIR spectra of *C. sinensis* polyphenol-mediated FeO NPs and *M. spicata* polyphenol-mediated FeO NPs.

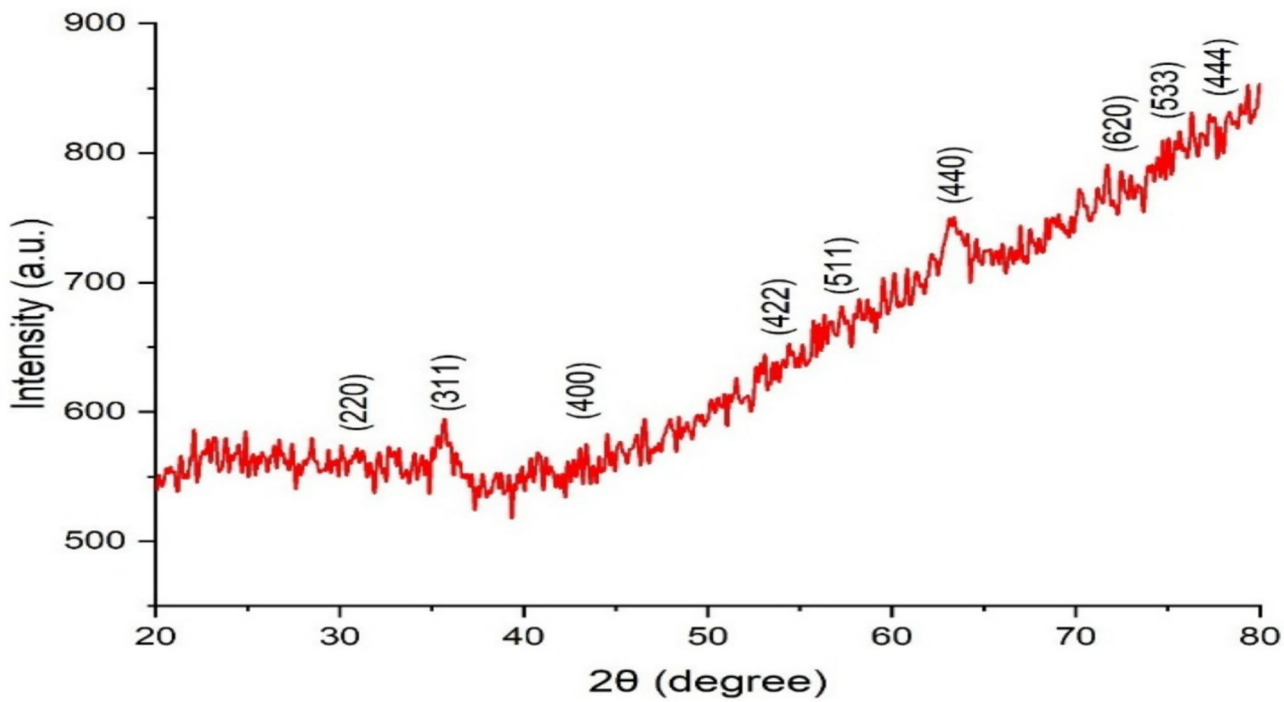

Fig. 4. XRD spectrum of *C. sinensis* polyphenol-mediated FeO NPs.

of FeO NPs was carried out using *M. spicata* polyphenols. The as-synthesized NPs were stored in sterile conditions for further characterization.

Characterization

The absorbance of FeO NPs fabricated using *C. sinensis* and *M. spicata* polyphenols was estimated using a Biospec-nano Spectrophotometer (206-26300-48; Shimadzu). A Fourier-transform infrared (FTIR; Miracle10; SHIMADZU) spectrophotometer was employed to scan the FeO NPs fabricated using *C. sinensis* and *M. spicata* polyphenols between the wavelengths of 4000 cm^{-1} and 400 cm^{-1}. The crystalline phase and structure of the FeO NPs were examined using an X-ray diffractometer (XRD; X'Pert Pro; PANalytical), while their shape was

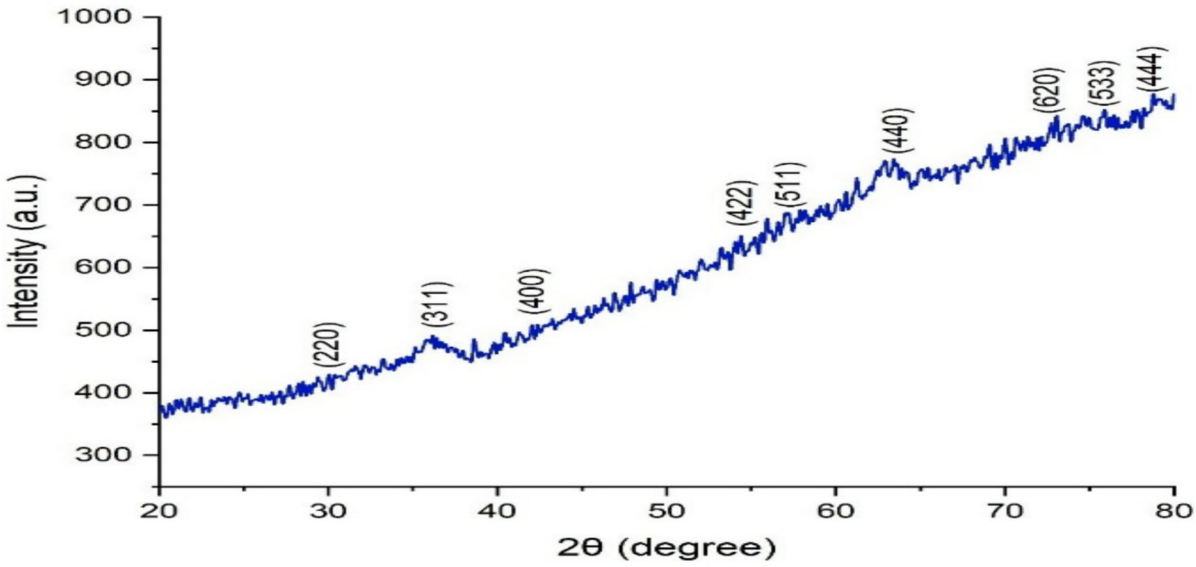

Fig. 5. XRD spectrum of *M. spicata* polyphenol-mediated FeO NPs.

determined using a field-emission scanning electron microscope (SEM; MIRA3 XMU; TESCAN)) with EDX analysis to confirm the elemental composition of the FeO NPs. Thermogravimetric analysis (TGA; EXSTAR/6300) was utilized to find the thermal stability of the FeO NPs.

RESULTS AND DISCUSSION

Phytochemical Screening and Total Phenolic Content

Table I shows the bioactive compounds of the *C. sinensis* and *M. spicata* aqueous extracts. Phytochemicals such as tannins, phenols, reducing sugars, flavonoids and sterol were present in the *C. sinensis* aqueous extract, while other phytochemicals such as saponins and glycosides were absent. Phytochemicals like tannins, phenols, flavonoids, glycosides and saponins were found in the *M. spicata* aqueous extract, while other phytochemicals such as sterol and reducing sugars were absent.

The total phenolic content of the *C. sinensis* polyphenol extract was 29.56 mg/ml GAE and for the for the *M. spicata* polyphenol was 28.56 mg/ml GAE.

Characterization

UV Visible Spectroscopy

The UV-Vis spectra of the *C. sinensis* polyphenol-mediated FeO NPs revealed maximum absorption at 230 nm (Fig. 1a) due to the surface plasmon resonance of the FeO NPs. Similarly, the UV-Vis spectra of *Murraya koenigii* showed maximum absorption peaks at 225 nm and 297 nm, indicating the formation of FeO NPs.[40] The UV-Vis spectrum (Fig. 2a) of *M. spicata* polyphenol-mediated FeO NPs displayed a maximum absorption at 250 nm, indicating the presence of FeO NPs. The strong absorption band observed in the UV region of *C. sinensis* polyphenol-mediated FeO NPs and the *M. spicata* polyphenol-mediated FeO NPs suggested that ligand-to-metal charge transition occurred within the Fe-O lattice. Tauc plots of the *C. sinensis* polyphenol-mediated FeO NPs (Fig. 1b) and *M. spicata* polyphenol-mediated FeO NPs (Fig. 2b) displayed a surface plasmon resonance. Wang et al.[41] synthesized FeO NPs using *Eucalyptus tereticornis* and observed a peak at 300 nm in the UV spectra. Abdullah et al.[42] reported that *Phoenix dactylifera* L.-mediated FeO NPs showed N absorption peak at 300 nm.

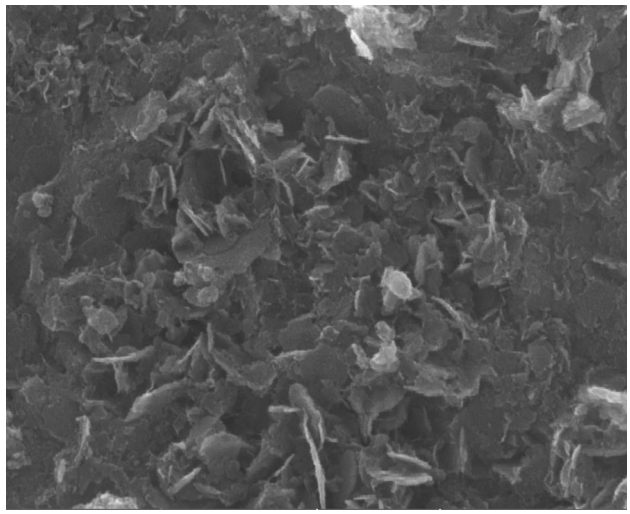

Fig. 6. FESEM image of *C. sinensis* polyphenol-mediated FeO NPs.

FTIR Analysis

Figure 3 depicts the infrared spectrum of the synthesized *C. sinensis* polyphenol-mediated FeO NPs. The spectrum represents various kinds of chemical bonds and their functional groups, and exhibits significant peaks at 956, 563, 493, and 432 cm^{-1}. The presence of these peaks indicates various molecular vibrations corresponding to specific functional groups. The peak at 956 cm^{-1} is attributed to alkyl and aryl halides, specifically C-H out-of-plane bending vibrations. Similarly, the peaks at 563, 493, and 432 cm^{-1} correspond to alkyl and aryl halides, with Br stretching and C-L stretching vibrations, respectively. Notably, the peak at 563 cm^{-1} signifies metal–oxygen vibrations, while the peaks at 493 and 432 cm^{-1} correspond to metal–ligand interactions. These spectral features strongly suggest the presence of polyphenolic compounds, including carbohydrates and tannins, along with an abundance of iron (Fe) ions, further confirming the complexation between plant metabolites and metal ions in the solution. The absorption bands at 446 and 531 cm^{-1} signify the vibrations of the Fe-O stretching bond, which confirms the presence of α-Fe_2O_3.[43]

The FTIR spectrum in Fig. 3 exhibits several absorption peaks at 3919, 3780, 3734, 3062, 2993, 2947, 1512, 1072, 856, 671, 555, 455, and 416 cm^{-1} indicating the presence of various functional groups. The broad peaks at 3919, 3780, and 3734 cm^{-1} are attributed to O-H stretching vibrations, indicating the presence of hydroxyl groups. The presence of aromatic compounds is verified by the peak at 3062 cm^{-1}, while the peaks at 2993 and 2947 cm^{-1} establish the C-H stretching vibrations of alkanes, indicating the presence of alkyl chains. The peak at 1512 cm^{-1} validated the presence of aromatic rings. Additionally, the peak at 1072 cm^{-1} is distinctive to ketones, indicating the presence of carbonyl groups. A specific peak at 856 cm^{-1} validated the presence of aromatic compounds. The FTIR spectrum also confirmed the occurrence of metal–oxide groups, from the peaks at 671, 555, 455, and 416 cm^{-1}. The FTIR spectrum of *Mentha piperita* polyphenol-mediated FeO NPs revealed distinct peaks at 587, 566 and 543 cm^{-1} suggesting the occurrence of metal-oxide functional groups.[43]

XRD Analysis

The crystallinity and phase purity of the synthesized FeO NPs were assessed XRD, and the XRD spectra in Fig. 4 show that the *C. sinensis* polyphenol-mediated FeO NPs were crystalline in nature, and their estimated size was 21.68 nm calculated using the Scherrer equation.

The XRD pattern of the sample shows the high crystallinity due to the sharp peaks obtained at 2θ of 30.46°, 35.86°, 43.46°, 57.46°, and 63.14° as per the ASTM standard for α-Fe_2O_3 NPs. A series of characteristic peaks were observed in the XRD pattern

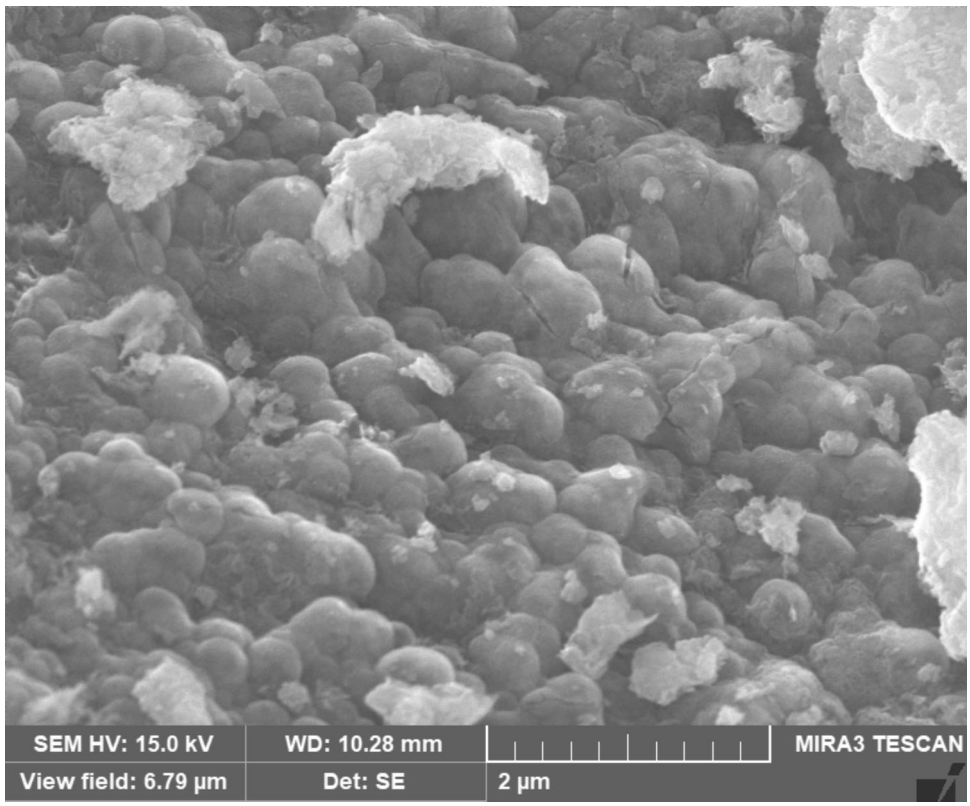

Fig. 7. FESEM image of *M. spicata* polyphenol-mediated FeO NPs.

at 2θ of 9.6°, 30.1°, 35.5°, 43.1°, 54.5°, 57.6°, and 63.6° corresponding to the diffractions of 220°, 311°, 400°, 422°, 511°, and 440° crystal phases of the Fe_3O_4 spinel structure, indicating the existence of magnetite NPs.[44] The XRD spectrum (Fig. 5) of the *M. spicata*-mediated FeO NPs shows peaks at (220), (311), (400), (422), (511), (440), (620), (533), and (444). The exhibited peaks with broad full-width at half-maxima indicate predominantly the crystalline nature of the *M. spicata*-mediated FeO NPs. The particle size of the NPs was calculated using Scherrer's formula, and was approximately 12.19 nm. The XRD spectra of the *C. sinensis* polyphenol-mediated FeO NPs validated that the phase of α-Fe_2O_3 was hematite with JCPDS ID 33-0664.[45]

FESEM Analysis

Figure 6 displays the FESEM image of *C. sinensis* polyphenol-mediated FeO NPs, which were nano-petal in shape, and their average size was 24–34 nm. Figure 7 displays the FESEM images of *M. spicata* polyphenol-mediated FeO NPs, which were spherical in shape, and their average was 20–28 nm. The polyphenol composition directly influences the shape of the nanoparticles by acting as a reducing, capping, and stabilizing agent. The molecular structure of the polyphenols and the types of functional groups are involved in activating various binding mechanisms. Different interactions such as electrostatic forces, hydrogen binding, and π–π interactions lead to the formation of the nano-petal and spherical morphology of the synthesized FeO NPs. The *C. sinensis*

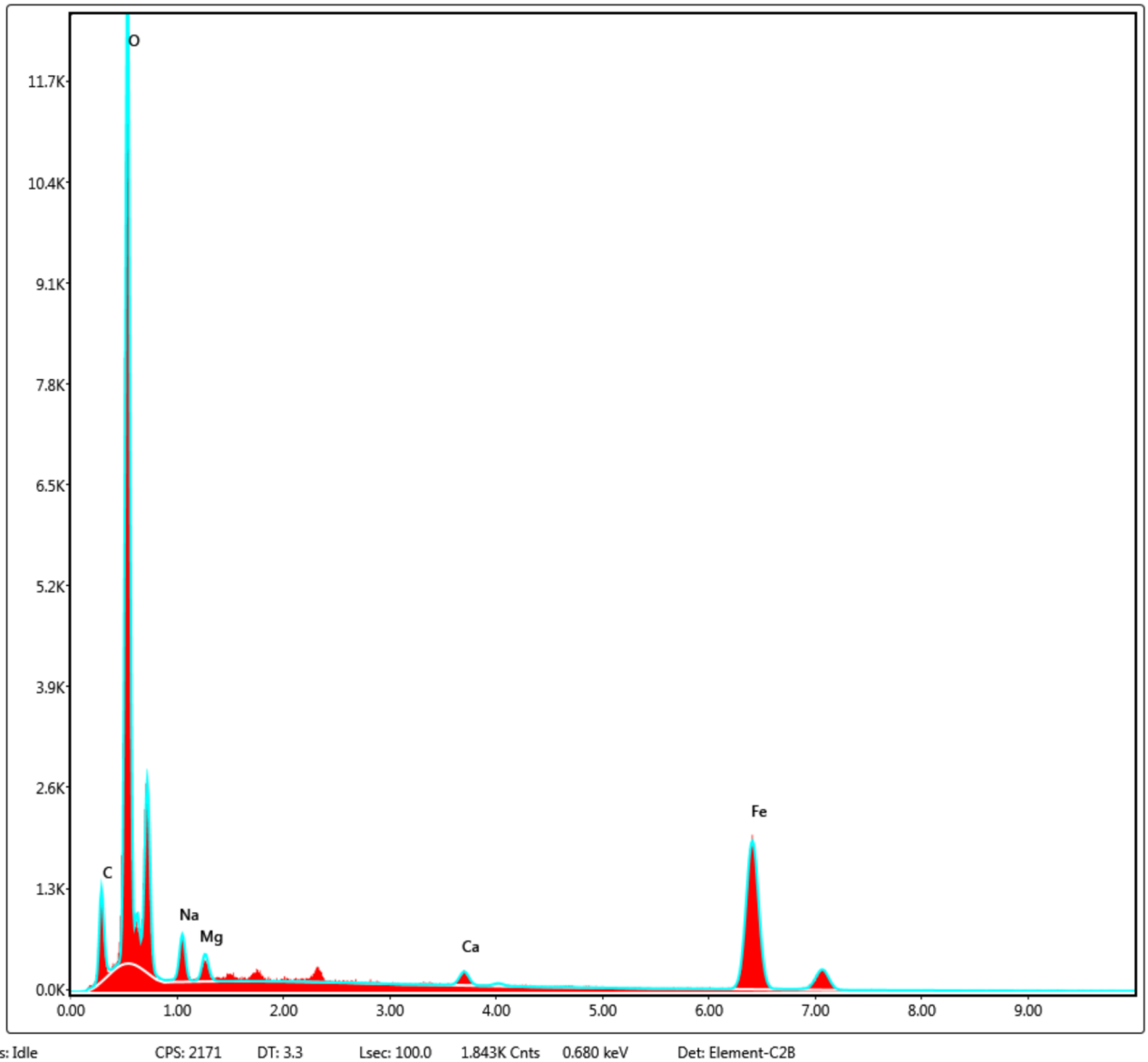

Fig. 8. EDX spectra of *C. sinensis* polyphenol-mediated FeO NPs.

polyphenol-mediated FeO NPs were larger in size due to their varied polyphenol composition and different binding mechanisms. The FESEM image of *Plumeria obtusa*-mediated FeO NPs confirmed that the NPs exhibited a well-defined morphology, with diameters ranging between 10 and 30 nm.[46] Mahdavi et al.[47] reported the cubic shape of Fe_3O_4 NPs using SEM images.

EDX Analysis

Figure 8 shows the EDX spectrum of *C. sinensis* polyphenol-mediated FeO NPs, which confirms the occurrence of iron, oxygen, carbon, sodium, magnesium, and calcium in both polyphenol-mediated FeO NPs. The *C. sinensis* polyphenol-mediated FeO NPs contained 51.64% of iron (Fe) and 34.20% of oxygen (O), while the *M. spicata* polyphenol-mediated FeO NPs (Fig. 9) contained 55% of iron (Fe) and 25% of oxygen (O). As expected, the peaks observed at approximately 0.8, 6.3, and 6.8 keV correspond to the binding energies of Fe. The spectrum reveals three distinct peaks attributed to Fe, O, and C. The presence of a carbon peak indicates the existence of biomolecules on the surface of the FeO NPs. EDX analysis revealed that *Eichhornia*-mediated FeO NPs consist of 77.08% iron and 22.97% oxygen.[48] The EDX spectrum displays iron and oxygen peaks, verifying the presence of the Fe_3O_4 phase without any impurities[1]

Thermogravimetric Analysis (TGA)

The TGA curve of the *C. sinensis* polyphenol-mediated FeO NPs (Fig. 10) revealed two major weight losses, of 18.1% and 12.9%, at 400 °C and

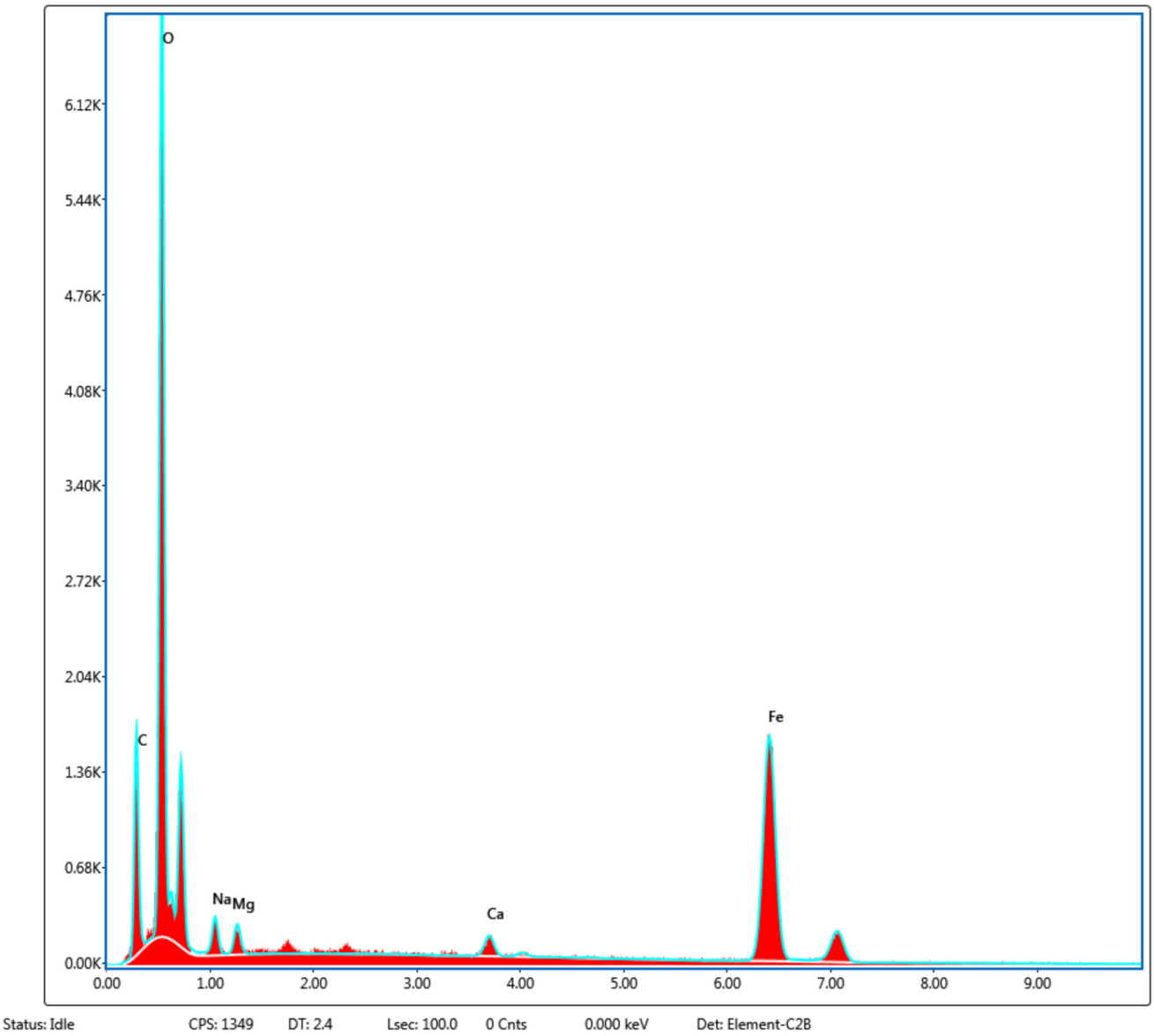

Fig. 9. EDX spectra of *M. spicata* polyphenol-mediated FeO NPs.

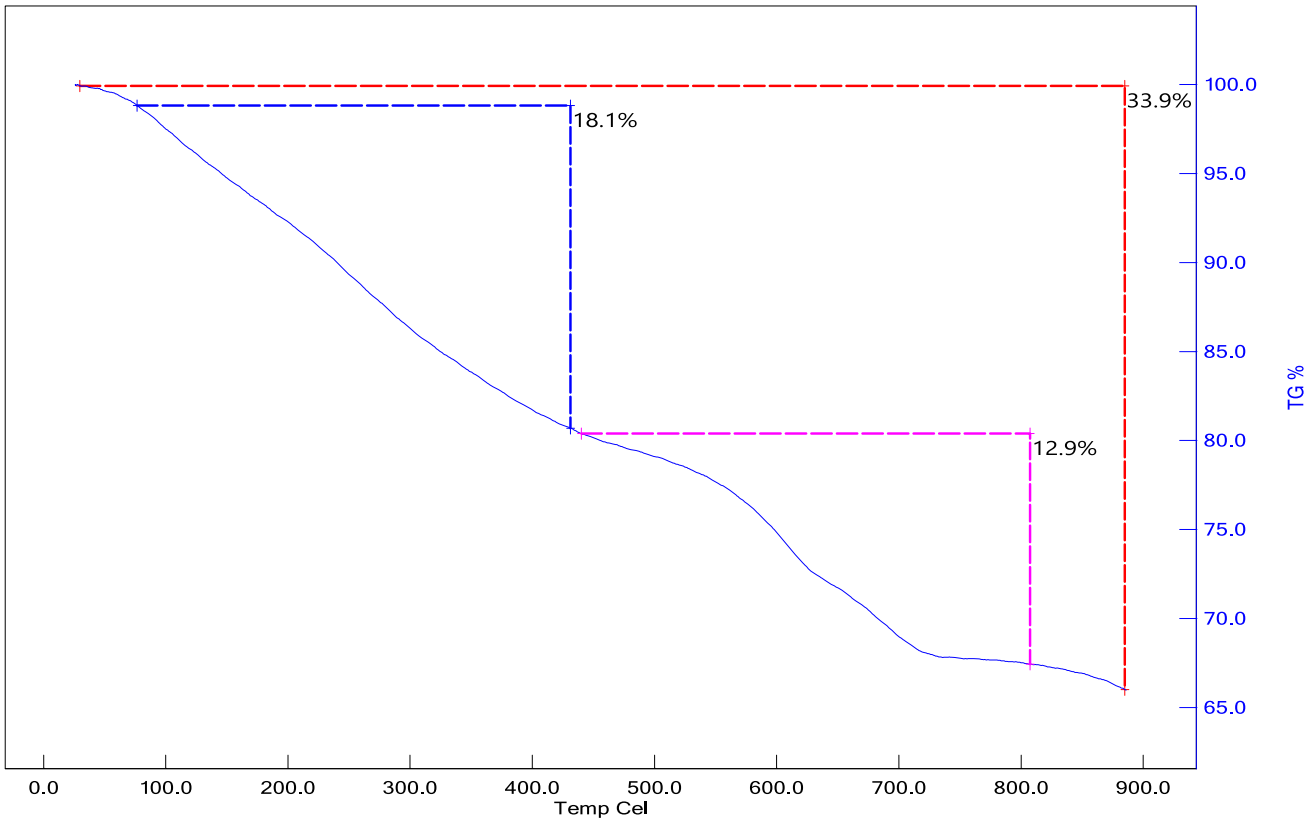

Fig. 10. TG analysis of *C. sinensis* polyphenol-mediated FeO NPs.

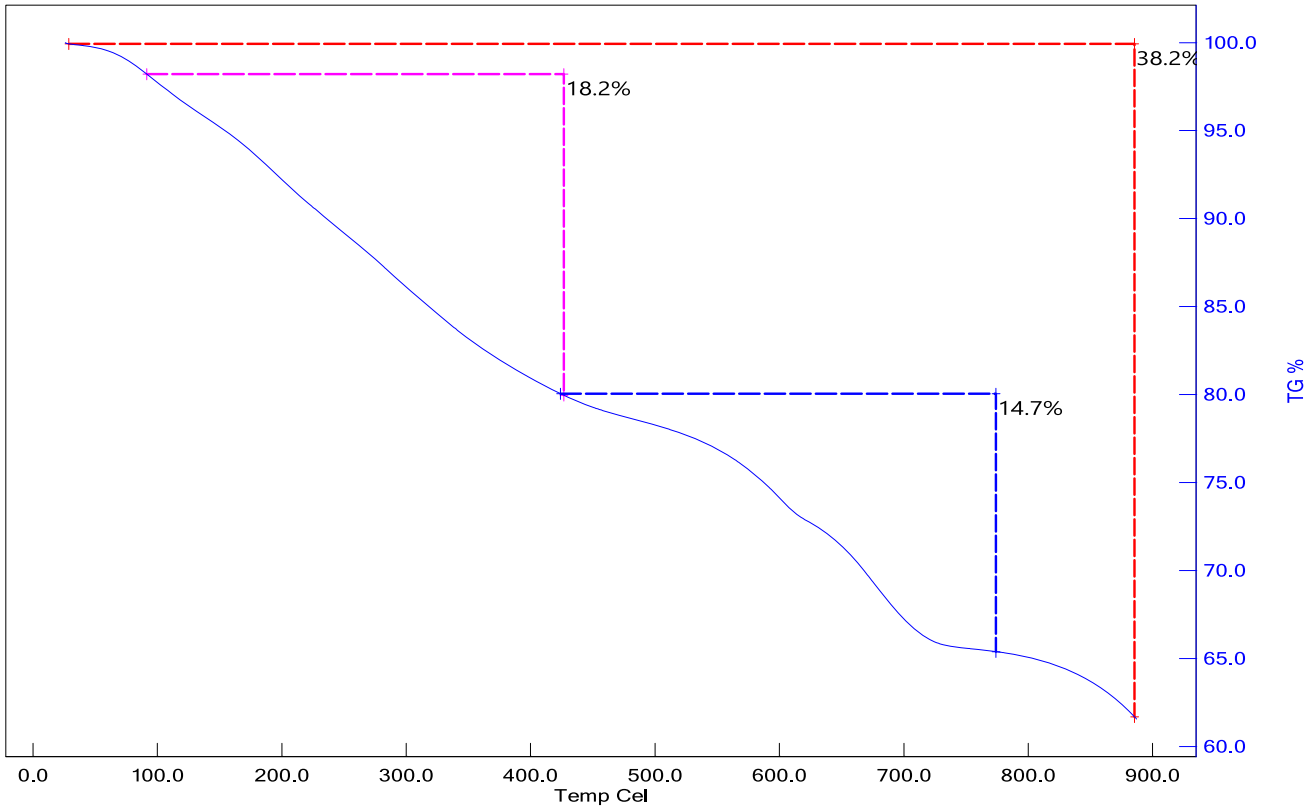

Fig. 11. TG analysis of *M. spicata* polyphenol-mediated FeO NPs.

Table II. Comparative study of FeO NPs

Properties	*C. sinensis* polyphenol-mediated FeO NPs	*M. spicata* polyphenol-mediated FeO NPs	*Punica granatum* polyphenol-mediated FeO NPs[51]
Functional group composition	Alkyl and aryl halides, metal oxides	Alcohols, aromatic compounds, alkanes and metal oxides	Alcohols, ketones, polyphenols, carboxylic acids
Crystallinity	Crystalline	Crystalline	Crystalline
Size	24–34 nm	20–28 nm	8.1 nm
Shape	Nano petal	Spherical	Quasi-spherical shape

800 °C, respectively. A total weight loss of 33.9 % occurred, indicating the loss of water molecules and low molecular weight compounds. Rami et al.[49] observed the TGA spectra of FeO NPs and confirmed that a slight weight fluctuation below 200 °C can be attributed to the evaporation of residual and adsorbed water molecules. This suggests that the biomolecule compounds coating the NPs possess thermal stability at lower temperatures, but begin to decompose and degrade at higher temperatures.[34] The TGA profile (Fig. 11) of *M. spicata* exhibited a total weight loss of 38.2%. The decomposition profile revealed a multi-stage process, with distinct temperature-dependent transitions. The initial thermal degradation was 18.2% at 400 °C, followed by rapid decomposition of 14.7% at 800 °C. The TGA data show a weight loss of the NPs up to 900 °C, due to the evaporation of water and organics. A mass loss was observed in the temperature range of 110–152 °C due to water evaporation, and this loss continued until the temperature reached 765 °C. The synthesized FeO NPs showed similar thermal degradation behavior, but *C. sinensis* showed slightly higher thermal stability due to its different polyphenol composition compared with *M. spicata*. Kayani et al.[50] performed TGA analysis and observed a mass reduction which was attributed to the loss of hydration water from the crystalline FeO NPs. Table II displays the comparative sizes, shapes, and nature of the FeO NPs synthesized using three different polyphenol sources. Polyphenols are bioactive compounds with various advantages in drugs and healthcare, and can be utilized as suitable capping agents for the fabrication of NPs. Further studies could be performed to utilize polyphenols for targeted therapies in healthcare and also for various environmental applications as photocatalysts and in wastewater treatment.

CONCLUSION

FeO NPs were synthesized using polyphenols of *C. sinensis* and *M. spicata* through a green chemistry approach. The physicochemical characteristics of the synthesized FeO NPs were evaluated using UV-Vis spectroscopy, FTIR, XRD, FESEM, EDX, and TGA analyses. The UV-Vis analysis of the polyphenol-mediated FeO NPs showed maximum absorption between 230 nm and 250 nm and proved the formation of an Fe-O lattice. The FTIR spectra of both polyphenol-mediated FeO NPs showed the presence of functional groups like alkyl and aryl halides and metal–oxygen groups. XRD analysis revealed the crystalline nature of both the polyphenol-mediated FeO NPs, while FESEM images showed that *C. sinensis* polyphenol-mediated FeO NPs were nano-petal in shape and *M. spicata* polyphenol-mediated FeO NPs were spherical in shape. The EDX spectra proved the presence of iron and oxygen in both the polyphenol-mediated FeO NPs. The *C. sinensis* polyphenol-mediated FeO NPs were thermally stable compared to *M. spicata* polyphenol-mediated FeO NPs.

AUTHOR CONTRIBUTIONS

Dr. Rajiv Periakaruppan: Conceptualization, Supervision, Administration; Ms. Nanditha Krishna S V: Investigation, Original draft; Mr. Jefri Samuel V: Investigation, Original draft; Mr. Joaval Antony Martin: Revision and Reviewing; Ms. Danusree Babu**:** Revision and Reviewing; Dr. Karungan Selvaraj Vijai Selvaraj: Revision and Reviewing; Dr. Noura Al-Dayan: Data Curation.

FUNDING

The authors have no relevant financial or non-financial interests to disclose.

CONFLICTS OF INTEREST

The authors declare that they have no conflict of interest.

REFERENCES

1. M. V. Arularasu, et al. An innovative approach for green synthesis of iron oxide nanoparticles: Characterization and its photocatalytic activity. Polyhedron, **155**, 287 (2018).
2. R. Zein, W. Sharrouf, and K. Selting, *J. Oncol.* 2020(1), 5194780 (2020).
3. N. Joudeh, and D. Linke, *J. Nanobiotechnology* 20(1), 262 (2022).
4. V. Pachkawade and Z. Tse, *Eng. Res. Express* 4(2), 022002 (2022).
5. X. Hu, Y. Zhang, T. Ding, J. Liu, and H. Zhao, *Front. Bioeng. Biotechnol.* 8, 990 (2020).
6. H.W. Tan, J. An, C.K. Chua, and T. Tran, *Adv. Electron. Mater.* 5(5), 1800831 (2019).

7. R. Abdul Rani, A.S. Zoolfakar, M.F. Mohamad Ryeeshyam, A.S. Ismail, M.H. Mamat, S. Alrokayan, H. Khan, K. Kalantar-zadeh, and M.R. Mahmood, *J. Electron. Mater.* 48, 3805 (2019).
8. J. Hong, C. Wang, D.C. Wagner, J.L. Gardea-Torresdey, F. He, and C.M. Rico, *Environ. Sci. Nano* 8(5), 1196 (2021).
9. A. Campos, N. Troc, E. Cottancin, M. Pellarin, H.C. Weissker, J. Lermé, M. Kociak, and M. Hillenkamp, *Nat. Phys.* 15(3), 275 (2019).
10. G. Cassone, *The journal of physical chemistry letters* 11(21), 8983 (2020).
11. A. Tufani, A. Qureshi, and J.H. Niazi, *Mater. Sci. Eng. C. Mater. Biol. Appl.* 118, 111545 (2021).
12. G. Li, Y. Sun, Q. Zhang, Z. Gao, W. Sun, and X. Zhou, *Chem. Eng. J.* 410, 128397 (2021).
13. M. Rahbar, A. Morsali, M.R. Bozorgmehr, and S.A. Beyramabadi, *J. Mol. Liq.* 302, 112495 (2020).
14. R. Saha, B. Mondal, and P.S. Mukherjee, *Chem. Rev.* 122(14), 12244 (2022).
15. C.G. Fraga, K.D. Croft, D.O. Kennedy, and F.A. Tomás-Barberán, *Food Funct.* 10(2), 514 (2019).
16. S.K. Garg, A. Shukla, and S. Choudhury 2019. Polyphenols and flavonoids. Nutraceuticals in veterinary medicine. pp.187–204.
17. N. Kumar and N. Goel, *Biotechnol. Rep.* 24, e00370 (2019).
18. S. Soleymani, S. Habtemariam, R. Rahimi, and S.M. Nabavi, *Trends Food Sci. Technol.* 106, 382 (2020).
19. J.M. Al-Khayri, R. Mascarenhas, H.M. Harish, Y. Gowda, V.V. Lakshmaiah, P. Nagella, M.Q. Al-Mssallem, F.M. Alessa, M.I. Almaghasla, and A.A.S. Rezk, *Molecules* 28(9), 3786 (2023).
20. D.D. Milinčić, D.A. Popović, S.M. Lević, A.Ž Kostić, ŽL. Tešić, V.A. Nedović, and M.B. Pešić, *Nanomaterials* 9(11), 1629 (2019).
21. J. Zhou, Z. Lin, Y. Ju, M.A. Rahim, J.J. Richardson, and F. Caruso, *Acc. Chem. Res.* 53(7), 1269 (2020).
22. X. Wang, Y. Fan, J. Yan, and M. Yang, *Chem. Eng. J.* 439, 135661 (2022).
23. Q. Dai, H. Geng, Q. Yu, J. Hao, and J. Cui, *Theranostics* 9(11), 3170 (2019).
24. T.H. Tran, N.T. Nguyen, and P.H. Dang. Evaluating phenolic compounds and antioxidant activity of the pericarps and seed coats extracts of Macadamia integrifolia and preparing their nanoemulsions (2023).
25. J. Xu, M. Wang, J. Zhao, Y.H. Wang, Q. Tang, and I.A. Khan, *Food Res. Int.* 107, 567 (2018).
26. A. Parveen, C.Y. Qin, F. Zhou, G. Lai, P. Long, M. Zhu, J. Ke, and L. Zhang, *Horticulturae* 9(12), 1253 (2023).
27. M. Cañellas-Santos, E. Rosell-Vives, L. Montell, A. Bilbao, F. Goñi-de-Cerio, and F. Fernandez-Campos, *Curr. Issues Mol. Biol.* 45(5), 3997 (2023).
28. D. Chen, Y. Ding, G. Chen, Y. Sun, X. Zeng, and H. Ye, *Food Res. Int.* 132, 109100 (2020).
29. S. Samanta, *Journal of the American Nutrition Association* 41(1), 65 (2022).
30. Y. Wang, Z. Kan, H.J. Thompson, T. Ling, C.T. Ho, D. Li, and X. Wan, *J. Agric. Food Chem.* 67(19), 5423 (2018).
31. M. Soleimani, A. Arzani, V. Arzani, and T.H. Roberts, *J. Herbal Med.* 36, 100604 (2022).
32. N. Brown, J.A. John, and F. Shahidi, *Food Production, Processing and Nutrition* 1(1), 1 (2019).
33. M.B. Bahadori, G. Zengin, S. Bahadori, L. Dinparast, and N. Movahhedin, *Int. J. Food Prop.* 21(1), 183 (2018).
34. K. Dhaouadi, M. Belkhir, F. Raboudi, E. Mecha, I. Ghommeme, M.D.R. Bronze, H. Ammar, and S. Fattouch, *J. Food Sci. Technol.* 53, 1164 (2016).
35. D. Letchumanan, S.P. Sok, S. Ibrahim, N.H. Nagoor, and N.M. Arshad, *Biomolecules* 11(4), 564 (2021).
36. K. Sen and S. Mondal, *Inorg. Chem. Commun.* https://doi.org/10.1016/j.inoche.2025.114682 (2025).
37. M. Jiménez-Rosado, A. Gomez-Zavaglia, A. Guerrero, and A. Romero, *J. Clean. Prod.* 350, 131541 (2022).
38. A. Rana, N. Kumari, M. Tyagi, and S. Jagadevan, *Chem. Eng. J.* 347, 91 (2018).
39. O. Dóka, G. Ficzek, G. Simon, Z. Zsófi, S. Villangó, and G. Végvári, *OENO One* 57(2), 257 (2023).
40. C.P. Devatha, A.K. Thalla, and S.Y. Katte, *J. Clean. Prod.* 139, 1425 (2016).
41. Z. Wang, C. Fang and M. Megharaj, *ACS Sustainable Chem. Eng.* 2(4), 1022 (2014).
42. J.A.A. Abdullah, L.S. Eddine, B. Abderrhmane, M. Alonso-González, A. Guerrero, and A. Romero, *Sustain. Chem. Pharm.* 17, 100280 (2020).
43. F.A. Shtewi, W.M. Barag, and A.A. Tarroush, *International Science and Technology Journal* 24, 355 (2021).
44. N. Ndou, T. Rakgotho, M. Nkuna, I.Z. Doumbia, T. Mulaudzi, and R.F. Ajayi, *Plants* 12(7), 1425 (2023).
45. R.T. Franco, A.L. Silva, Y.E. Licea, J.D. Serna, M. Alzamora, D.R. Sánchez, and N.M. Carvalho, *Inorg. Chem.* 60(8), 5734 (2021).
46. S. Perveen, R. Nadeem, S. ur Rehman, N. Afzal, S. Anjum, S. Noreen, R. Saeed, M. Amami, S.H. Al-Mijalli, and M. Iqbal, *Arab. J. Chem.* 15(5), 103764 (2022).
47. M. Mahdavi, et al., *Molecules* 18(7), 7533 https://doi.org/10.3390/molecules18077533 (2013).
48. G. Jagathesan, and P. Rajiv, *Biocatal. Agric. Biotechnol.* 13, 90 (2018).
49. J.M. Rami, et al. Thermogravimetric analysis (TGA) of some synthesized metal oxide nanoparticles. [Molecular Pharmaceutics]. (2005) https://doi.org/10.1021/mp0500014.
50. Z.N. Kayani, S. Arshad, S. Riaz, and S. Naseem, *IEEE Trans. Magn.* 50(8), 1 (2014).
51. A.E. Matías-Reyes, M.L. Alvarado-Noguez, M. Pérez-González, M.D. Carbajal-Tinoco, E. Estrada-Muñiz, J.A. Fuentes-García, L. Vega-Loyo, S.A. Tomás, G.F. Goya, and J. Santoyo-Salazar, *Nanomaterials* 13(17), 2450 (2023).